# The TiNiSi Family of Compounds: Structure and Bonding

**Gregory A. Landrum[†] and Roald Hoffmann***

Department of Chemistry and Materials Science Center, Cornell University, Ithaca, New York, 14853-1301

**Jürgen Evers***

Institut für Anorganische Chemie, Universität München, Meiserstr. 1, D-80333 München, Germany

**Hans Boysen**

Institut für Kristallographie, Universität München, Theresienstr. 41, D-80333 München, Germany

*Received February 27, 1998*

We report the synthesis and structure and discuss in substantial detail the bonding of a remarkable family of compounds spanning most of the transition series. All members of the MTSi (M = Sc, Ti, V, Cr, Mn, Fe, Co, Ni; T = Co, Ni) series have now been prepared, and their crystal structures have been determined accurately using X-ray diffraction and, for MnNiSi and FeNiSi, neutron diffraction. Each of these compounds, four of which were previously unknown, crystallizes in the TiNiSi structure type. In contrast, for T = Cu, one has only representatives with M = Sc and Ti. A simple Zintl picture, which works so well for the three-dimensional four-connected indium net of the related $BaIn_2$ structure, is not applicable to these intermetallics; there is substantial M−T and M−Si bonding, and the "extra" electrons in the MTSi structure enter orbitals essentially nonbonding within the TSi network. A structural change observed for M = Fe and higher d-electron counts, distorting the six-rings in the structure, is traced to the formation of M−M bonds. The instability of the corresponding Cu phases is discussed in terms of Miedema's ideas about electronegativity and electron density.

## 1. Introduction

The TiNiSi (or $Co_2Si$) structure type (space group *Pnma*, Pearson symbol oP12) is a lower symmetry relative of the $CeCu_2$ structure (space group *Imma*). In a previous publication, we presented a detailed analysis of the bonding in the $CeCu_2$ structure type.[1] While $CeCu_2$ is quite a common structure, with 81 known examples as of 1991,[2] the TiNiSi structure type is even more versatile; 495 manifestations are reported in the same publication. There are strong similarities between the two structure types. Both TiNiSi and $CeCu_2$ have three-dimensional four-connected (3D4C) anionic networks with cations sitting in large channels. Both networks can be viewed as being composed of two-dimensional sheets of edge-sharing six-membered rings similar to those in black phosphorus running perpendicular to the $\vec{a}$ axis, **1**.

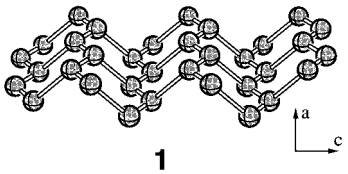


**1**

The six-ring sheets are linked along the $\vec{a}$ direction to form one-dimensional ladders of edge-sharing four-rings and channels of eight-rings running along $\vec{b}$. Figure 1 shows a side-by-side comparison of the anion networks of $BaIn_2$ (the member of the $CeCu_2$ family discussed in ref 1) and TiNiSi. The obvious difference between $BaIn_2$ and TiNiSi is the shape of the four-rings that make up the ladders. The rectangular ladders of $BaIn_2$ (**2**, left) are significantly tilted in TiNiSi (**2**, right).

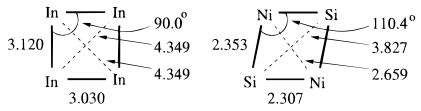


**2**

The electronic reasons behind this are actually quite simple; the rectangles tilt in order to move more electronegative Si atoms away from each other.[1] Despite the relatively close Ni−Ni contact, our calculations (not shown here) do not indicate that there is any significant Ni−Ni bond formation in this structure.

In our earlier work, we examined the bonding in the related, higher symmetry, $BaIn_2$ structure. We showed the utility of the Zintl view in combination with crystal orbital overlap population (COOP) curves for the prediction/explanation of stable members of the family. The Zintl approach used in our previous analysis relied upon being able to separate, for example, $BaIn_2$ into isolated $Ba^{2+}$ cations and an $In_2^{2-}$ network. The $In^-$ anions, which make up the $In_2^{2-}$ net, are isoelectronic to C, so the $In_2^{2-}$ network is four-connected. The basic network

* Corresponding author.
[†] Current address: Institut für Anorganische Chemie, RWTH−Aachen, Prof.-Pirlet-Str. 1, D-52074 Aachen, Germany.

(1) Nuspl, G.; Evers, J.; Landrum, G. A.; Hoffmann, R. *Inorg. Chem.* **1996**, *35*, 6922.
(2) Villars, P.; Calvert, L. D. *Pearson's Handbook of Crystallographic Data for Intermetallic Phases*, 2nd ed.; ASM International: OH, 1991.

10.1021/ic980223e CCC: $15.00 
Published on Web 10/08/1998

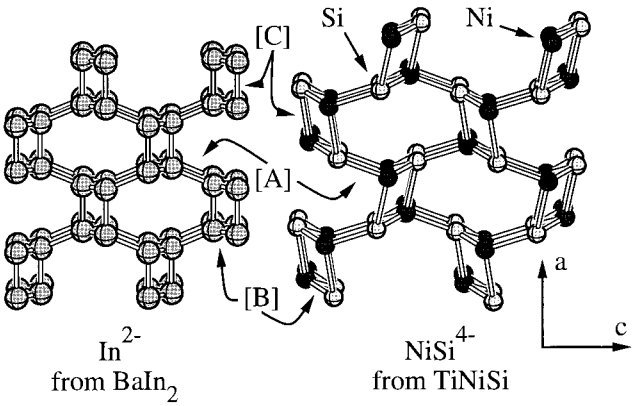


**Figure 1.** Views along $\vec{b}$ of the 3D4C networks of $BaIn_2$ and TiNiSi. The three symmetry-unique bonds within each network are labeled.

is stable for a wide range of electron counts, between 16 and 32 electrons per unit cell (two to four electrons per atom in the network).

The concern of this contribution is a particularly fascinating series of ternary MTX (M = transition metal, T = late transition metal, X = main group element) compounds in the TiNiSi structure type that has been prepared. Previously, MNiSi with M = Sc, Ti, V, and Ni and MCoSi with M = Sc and Ti have been prepared and structurally characterized.[2] Here, we present the structures of the remaining members of this family, which spans the entire first transition series. As well as being appealing on an intellectual level (How is it possible that one structure can be adopted for such a range of electron counts?), these compounds, all metallic conductors, exhibit a range of magnetic behaviors running from Pauli paramagnetism (M = Sc, Ti, V) through ferromagnetism (M = Cr, Mn, Fe). CoNiSi and NiNiSi also show strong magnetic properties, but the temperature dependence of their susceptibilities has not yet been determined.

We will examine the bonding in these phases in some detail in order to understand the observed structural trends. We will focus on three primary questions.

1. How can a single structure type accommodate so many different electron counts?

2. What electronic factors give rise to the observed changes in ring geometries and lattice constants (see below)?

3. Why is it that MCuSi phases can only be prepared for M = Sc and Ti?

## 2. Experimental Work

The two homologous series of ternary silicides MCoSi and MNiSi (M = Sc, Ti, V, Cr, Mn, Fe, Co, Ni) contain 15 members. Among these, the alphabetic listing of ternary phases with the TiNiSi structure, published in 1991, contains 11 ternary silicides of these series, while the remaining four silicides have not been reported with this structure.[2] However, the tabulated structural data for most of the 11 reported silicides were determined in the 1960's by low-resolution techniques, e.g., from Debye−Scherrer X-ray photographs. Only for CoCoSi (=$Co_2Si$), TiNiSi, and NiNiSi (=$Ni_2Si$) have single-crystal X-ray structures been determined. In addition, for one compound, MnCoSi, a neutron diffraction investigation was published.[3] The use of neutron diffraction to characterize these systems could be important because the X-ray scattering factors for nearly adjacent elements such as manganese and cobalt, with 25 and 27 electrons, respectively, do not differ significantly. This leads to lower resolution in the determination of positions with X-ray diffraction in comparison to neutron diffraction. In this earlier neutron diffraction study, two different samples of nominal composition MnCoSi were measured. However, the two sets of determined lattice and positional parameters differ significantly, perhaps due to a lack of homogeneity within the samples.

To obtain precise structural data on the MCoSi and MNiSi silicide series, three requirements had to be fulfilled: (1) preparation of high-purity, stoichiometric, and homogeneous polycrystalline samples, (2) determination of lattice and positional parameters with modern high-resolution X-ray powder diffraction (Guinier) techniques, (3) checking the results of X-ray investigations on a few samples composed of adjacent 3d elements using neutron powder diffraction.

In an inductively heated copper boat under an argon atmosphere, 15 MCoSi and MNiSi samples (1 g each) were prepared for X-ray diffraction by quasi-crucible-free melting. The first advantage of this method is that the opposed high currents running through the sample and the copper boat cause the sample to levitate above the boat, preventing wetting of the cold surface of the boat. The second advantage is that during melting the liquid samples are intensively stirred by electromagnetic forces. Starting materials were electronic grade silicon and metals of at least 99.9 wt % purity with respect to metallic impurities. For neutron diffraction, two samples (6 g each) of composition MnNiSi (Mn, $25e^-$; Ni, $28e^-$) and FeNiSi (Fe, $26e^-$; Ni, $28e^-$) were prepared in the copper boat by several single melting experiments. These samples were pulverized in a mill using corundum spheres.

X-ray structural investigations were performed using a Guinier diffractometer (Huber G 644) with monochromated molybdenum radiation in sealed capillaries (0.3 mm diameter). The diffractometer was calibrated with electronic grade germanium. The measured $2\theta$ range was between 8° and 38° with an increment of 0.04° and a counting rate of 60 s per increment. The 750 data points obtained were corrected for absorption. Two programs were used for Rietveld analyses of the X-ray Guinier diffractograms.[4,5]

Four new silicides in the series MCoSi and MNiSi with TiNiSi structure have been found: FeCoSi, CrNiSi, FeNiSi, and CoNiSi. Ten of the fifteen silicides were obtained as single-phase compounds with the TiNiSi structure, but five were only obtainable as phase mixtures. Additional melting experiments for these five silicides, as well as annealing experiments in evacuated, sealed silica tubes, did not improve their phase purity. MnNiSi consists of 95% of the main phase with the TiNiSi structure and 5% of an additional phase, which also has the TiNiSi structure but a unit cell volume that is 5% smaller than that of the main phase. In VCoSi, an additional TiNiSi phase is also found, composing 10% of the sample. FeCoSi is also a two-phase compound, 80% a main phase with the TiNiSi structure, and 20% of an additional phase with the ZrBeSi (ternary $Ni_2$ In) structure. CrCoSi is a three-phase mixture, containing 80% of the main TiNiSi phase, 15% of an additional TiNiSi phase, and 5% of a ZrBeSi phase. Finally, CrNiSi is a four-phase mixture (60% main TiNiSi phase, 20% a phase with the α-manganese structure, 15% of an additional TiNiSi phase, and 5% of a ZrBeSi phase).

Structural investigations with neutron radiation on MnNiSi and FeNiSi have been performed at the MAN2 diffractometer of the FRM reactor facility in Garching/Obb., Germany using a wavelength $\lambda$ = 1.1120 Å and an angular range $2\theta = 4°-110°$, with a step width of 0.1°. The data were evaluated with an extended version[6] of the Rietveld program PROF.[7] Nuclear scattering lengths were taken from the compilation of Koester, Rauch, and Seyman[8] (Fe, 9.45 fm; Mn, −3.7 fm; Ni, 10.3 fm; Si, 4.149 fm) and magnetic form factors from that of Brown.[9] Test refinements using form factors for different valencies yielded only insignificant differences.

(3) Binczycka, H.; Szytula, A.; Todorovic, J.; Zaleski, T.; Zieba, A. *Phys. Status Solidi A* **1976**, *35*, 69.

(4) Wiles, D. B.; Young, R. A. *Program for Rietveld Analysis of X-ray and Neutron Powder Diffraction Patterns (DBW 2.9)*; Georgia Institute of Technology: Atlanta, GA, 1982.

(5) Schneider, J. *Acta Crystallogr. A* **1987**, *43* (Suppl. C), 467.

(6) Boysen, H. In *Accuracy in Powder Diffraction II*; Prince, E., Stalick, J. K., Eds.; NIST Special Publication 846; Washington, 1992; p 165.

(7) Thomas, M. W.; Bendall, P. J. *Acta Crystallogr. A* **1978**, *34*, 351.

(8) Sears, V. F. *Neutron News* **1992**, *3*, 26.

(9) Brown, P. J. In *International Tables for Crystallography*; Wilson, A. J. C., Ed.; Kluwer Academic Publishers: Dordrecht, 1992; p 391.

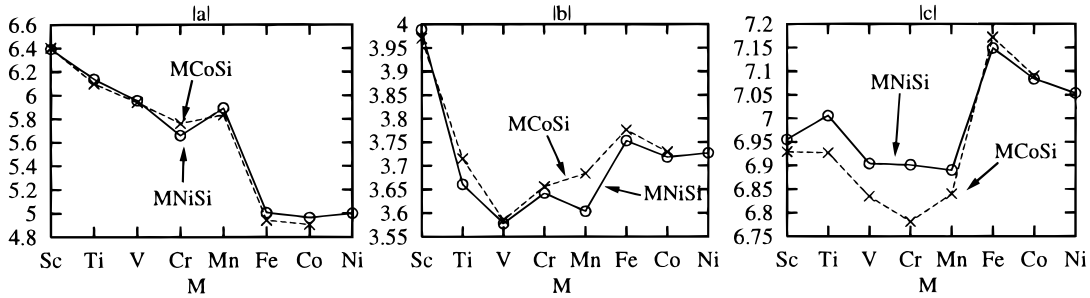


**Figure 2.** Lattice constants in the MNiSi (solid lines) and MCoSi (dashed lines) series plotted against M. All lengths are in angstroms.

**Table 1.** X-ray Diffraction Results for Seven MCoSi Compounds with the TiNiSi Structure[a]

| M | $\|a\|$ (Å) | $\|b\|$ (Å) | $\|c\|$ (Å) | %*A* (%) | $R_{wp}$ (%) | $R_{exp}$ (%) |
|---|---|---|---|---|---|---|
| Sc | 6.401(2) | 3.970(1) | 6.929(2) | 100 | 6.62 | 14.58 |
| Ti | 6.100(2) | 3.715(1) | 6.927(2) | 100 | 8.63 | 13.94 |
| V | 5.941(2) | 3.585(1) | 6.835(2) | 95 | 9.50 | 15.12 |
| Cr | 5.772(2) | 3.664(1) | 6.775(2) | 80 | 9.67 | 13.21 |
| Mn | 5.835(2) | 3.684(1) | 6.840(2) | 100 | 7.68 | 14.35 |
| Fe | 4.942(2) | 3.776(1) | 7.172(2) | 80 | 8.62 | 14.16 |
| Co | 4.906(2) | 3.729(1) | 7.090(2) | 100 | 6.92 | 14.50 |

[a] Lattice constants are for the main phase. %A refers to the percentage of the sample that was in the main TiNiSi phase.

**Table 2.** X-ray Diffraction Results for Seven MNiSi Compounds with the TiNiSi Structure[a]

| M | $\|a\|$ (Å) | $\|b\|$ (Å) | $\|c\|$ (Å) | %*A* (%) | $R_{wp}$ (%) | $R_{exp}$ (%) |
|---|---|---|---|---|---|---|
| Sc | 6.392(2) | 3.989(1) | 6.955(2) | 100 | 6.55 | 15.20 |
| Ti | 6.139(2) | 3.661(1) | 7.006(2) | 100 | 7.26 | 14.56 |
| V | 5.956(2) | 3.578(1) | 6.904(2) | 100 | 8.05 | 15.25 |
| Cr | 5.667(2) | 3.613(1) | 6.887(2) | 60 | 12.24 | 17.07 |
| Mn | 5.892(2) | 3.604(1) | 6.890(2) | 95 | 5.68 | 14.82 |
| | *5.892(1)* | *3.604(1)* | *6.897(1)* | *95* | *8.05* | 6.49 |
| Fe | 5.007(2) | 3.753(1) | 7.149(2) | 100 | 6.25 | 14.72 |
| | *5.007(1)* | *3.753(1)* | *7.149(1)* | *100* | *7.74* | 6.56 |
| Co | 4.964(2) | 3.718(1) | 7.084(2) | 100 | 5.76 | 15.32 |
| Ni | 5.001(2) | 3.727(1) | 7.054(2) | 100 | 5.90 | 15.35 |

[a] Lattice constants are for the main phase. %A refers to the percentage of the sample that was in the main TiNiSi phase. Numbers in italics for MnNiSi and FeNiSi were determined from the neutron diffraction study.

For FeNiSi, satisfactory agreement factors are obtained for a single-phase compound with nuclear scattering only. These may be further reduced by introducing a small magnetic moment for Fe ordered ferromagnetically along the $\vec{b}$ axis. Broad, diffuse humps in the background are indicative of short-range magnetic order. On the other hand, for MnNiSi, there are large magnetic contributions and the flat background indicates complete long-range order. Again the ordering is ferromagnetic, and the Mn moment is directed along the $\vec{b}$ axis. However, the use of only one phase left some extra reflections indicating the presence of some second phase (5%) also with the TiNiSi structure but with a 5% lower cell volume than the main phase. This is in agreement with the results of X-ray diffraction on MnNiSi.

In Tables 1 and 2, the lattice parameters, percentage of the main TiNiSi phase, and agreement factors ($R_{wp}$) between the observed and the calculated diffractograms, determined by X-ray diffraction, are presented for the MCoSi and MNiSi silicides, respectively. Table 2 also contains (in italics) the lattice parameters obtained from the neutron data. The positional parameters for all of the phases, as determined from the X-ray data, are given in the Supporting Information. In Table 3, the positional parameters, determined by both X-ray and neutron diffraction, for MnNiSi and FeNiSi are presented. Table 3 also presents the Mn and Fe magnetic moments for ferromagnetic ordering along the $\vec{b}$ axis as determined from the neutron experiments.

Inspection of the results for MnNiSi and FeNiSi in Tables 2 and 3 shows that there are only small differences between the lattice and positional parameters determined by X-ray and by neutron scattering.

**Table 3.** Positional Parameters and Magnetic Data for MnNiSi and FeNiSi in the TiNiSi Structure[a]

| | M | | Ni | | Si | | |
|---|---|---|---|---|---|---|---|
| M | *x* | *z* | *x* | *z* | *x* | *z* | $m/\mu_b$ |
| Mn | 0289(6) | 6733(4) | 1449(4) | 0595(4) | 2598(12) | 3703(7) | |
| | *0268(7)* | *6747(6)* | *1454(9)* | *0582(3)* | *2596(6)* | *3703(6)* | *2.61(6)* |
| Fe | 0425(8) | 7130(4) | 1726(6) | 0611(4) | 2022(15) | 3893(9) | |
| | *0438(3)* | *7147(3)* | *1739(5)* | *0614(3)* | *2129(13)* | *3899(7)* | *0.96(7)* |

[a] All atoms are in site 4c ($x$, $^1/_4$, $z$), space group *Pnma*. Positional parameters are for the main phase. Numbers in italics are from the neutron diffraction data. *m* is the measured magnetic moment in Bohr magnetons.

## 3. Structural Systematics

MNiSi in the TiNiSi structure have been identified for M = Sc, Ti, V, Cr, Mn, Fe, Co, and Ni. Crystal structures for all of these compounds have been determined. *This remarkable family of compounds spans the entire first transition series!* However, if we move T over just one column to the *right*, to give MCuSi, the situation is markedly different. MCuSi is only known for M = Sc, Ti. Attempts to prepare the other possible members of the family, using the same techniques which give the MNiSi compounds with little difficulty, have failed. This obviously cannot be merely a consequence of different electron counts; the nonexistent VCuSi phase would be isoelectronic to CrNiSi, which is known and stable. If, on the other hand, we move the T in MNiSi over one column to the *left*, the resulting MCoSi compounds once again span the entire first transition series: M = Sc, Ti, V, Cr, Mn, Fe, Co. So, while a simple electron counting scheme was sufficient to describe many of the binary members of the $CeCu_2$ family, things are more complicated for the MNiSi, MCoSi, and MCuSi series of compounds. This difference between the T = Ni, Co and T = Cu series will be addressed here.

The lattice constants of the MNiSi and MCoSi structures are plotted against M as we move across the first transition series in Figure 2. There are discontinuities in the curves for $|\vec{a}|$ and $|\vec{b}|$ in each series at M = Fe. These sharp changes are accompanied by a small but significant change in the structure of the TSi network. Figure 3 shows the NiSi networks of MnNiSi and FeNiSi. The six-rings in MnNiSi are in the chair form (really closer to a half-chair), just as they were in TiNiSi. FeNiSi is, however, different; the six-rings are in the boat form. To make this difference clearer, Figure 4 shows single six-rings from MNiSi structures with M = Sc,V, Mn, Fe, and Ni. This structural change persists through the rest of each series; FeNiSi, CoNiSi, NiNiSi, FeCoSi, and CoCoSi all have short $\vec{a}$ lattice parameters. This change is, once again, not a function of electron count; FeCoSi has the same number of valence electrons as MnNiSi, yet it has the same structural characteristics as FeNiSi. This effect, which must be due to the nature of M, will be examined below.

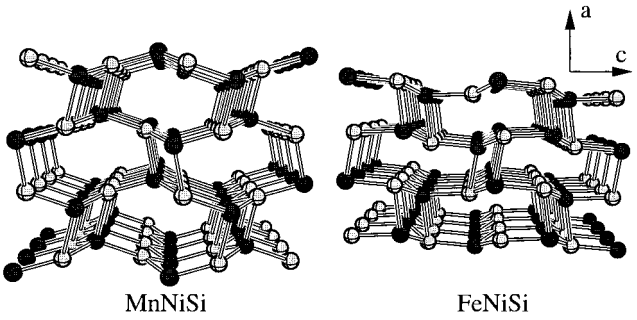


**Figure 3.** The NiSi networks of MnNiSi (left) and FeNiSi (right). The transformation between chair and boat form six-rings is visible, as is the contraction along the $\vec{a}$ direction.

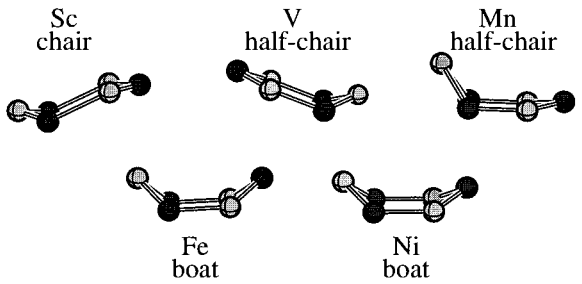


**Figure 4.** Six-membered rings cut from the structures of MNiSi compounds with M = Sc, V, Mn, Fe, and Ni.

## 4. Bonding in the TiNiSi Structure Type

A quick bit of electron counting provides the first sign that our simple Zintl scheme may not work for the MNiSi family. Using the same counting scheme as that used for $BaIn_2$, we arrive at a count of 32 electrons/cell in TiNiSi (Ti:4 + Ni:0 + Si:4 = 8 × 4 formula units/cell → 32 electrons/cell). We count the Ni as contributing zero valence electrons because, within this simple counting scheme, we ignore its full d block. Moving M over one column to obtain VNiSi, we obtain a valence electron count of 36 electrons/cell for VNiSi. Now, within our earlier view, the four-connected NiSi network should not be stable for a count of 36 electrons (32 electrons was the most that the $In_2$ network of $BaIn_2$ could accommodate). The network just cannot accommodate that many electrons without populating too many strongly antibonding levels. This situation raises the first question that we must address—What happens to the "extra" electrons in the later members of the MNiSi series?

We will be doing the majority of our analysis of the electronic structure and bonding of TiNiSi using the extended Hückel implementation of the tight-binding method (eHT).[10−16] Because the extended Hückel theory is a semiempirical method, there is always the nagging possibility that a bad parameter set is being used, rendering the results unreliable. To assuage these fears and provide more confidence in the results, we have also generated the electronic structure of TiNiSi using a more reliable theory, the linear muffin tin orbital (LMTO) method. [17−22] In Figure 5 the calculated total densities of states (DOSs) and Ti-projected DOSs from both eHT and LMTO are shown. To allow direct comparison of the two DOS curves, both have been shifted to place the Fermi level at 0 eV. There is remarkable agreement between the two DOS curves. The shapes and bandwidths (dispersions) of the total DOS- and Ti-projected DOS curves, both above and below $\epsilon_f$, are very similar.

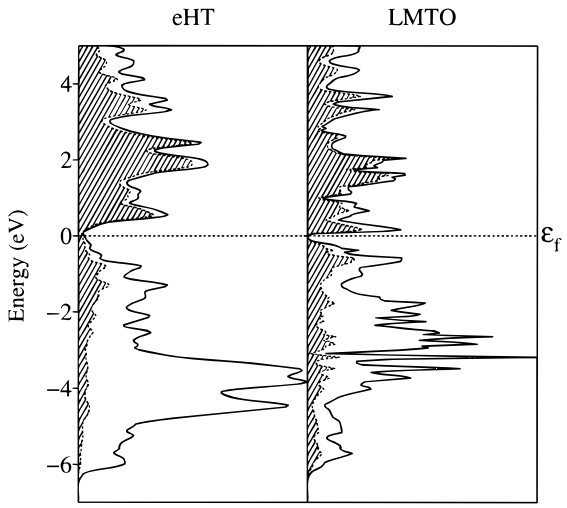


**Figure 5.** The total DOS (solid line) and Ti-projected DOS (dashed line) for TiNiSi calculated using extended Hückel theory (left) and the LMTO method (right). To facilitate comparison, both DOS curves have been shifted so that $\epsilon_f$ (the horizontal dotted line) is at 0 eV.

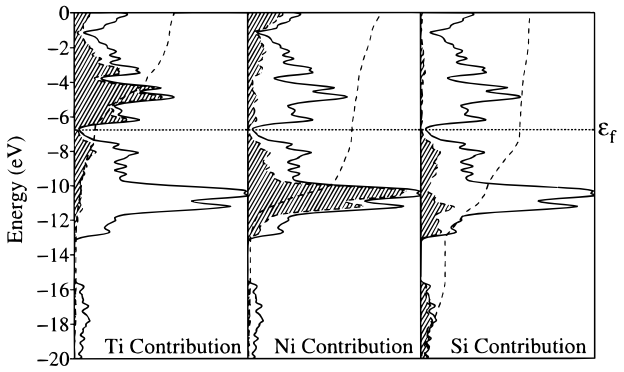


**Figure 6.** Projected DOS curves (shaded regions) for Ti (left), Ni (center), and Si (right) in TiNiSi. The dashed line in each curve is the integration of the projected states.

Now that we know we have a reasonable set of eHT parameters for TiNiSi (these parameters are given in the section below on computational details), we proceed with our analysis of the bonding in TiNiSi. Figure 6 shows the projected DOS curves for each of the three types of atoms that make up TiNiSi. The lowest-lying states in this energy window are primarily Si 3s orbitals. The large peak in the DOS between −11 and −10 eV is mostly made up of Ni 3d states. The low, broad peak between −13 and −7 eV, which has contributions from both Ni and Si toward the bottom and all three atom types toward the top, is likely where the bonding in TiNiSi is happening. The majority of the Ti states show up in the region of unfilled states just above $\epsilon_f$. This electron deficiency is responsible for the large positive charge on Ti, +1.88. The 1.88 electrons

(10) Hoffmann, R. *J. Chem. Phys.* **1963**, *39*, 1397.
(11) Hoffmann, R. *J. Chem. Phys.* **1964**, *40*, 2745.
(12) Hoffmann, R. *J. Chem. Phys.* **1964**, *40*, 2474.
(13) Whangbo, M.-H.; Hoffmann, R. *J. Am. Chem. Soc.* **1978**, *100*, 6093.
(14) Whangbo, M.-H.; Hoffmann, R.; Woodward, R. B. *Proc. R. Soc. London* **1979**, *A366*, 23.
(15) Ashcroft, N. W.; Mermin, N. D. *Solid State Physics*, Saunders College Publishing: New York, 1976.
(16) Hoffmann, R. *Solids and Surfaces: A Chemist's View of Bonding in Extended Structures*; VCH: Weinheim, 1988.
(17) Andersen, O. K. *Phys. Rev. B* **1975**, *12*, 3060.
(18) Andersen, O. K. *Europhys. News* **1981**, *12*, 4.
(19) Andersen, O. K. In *The Electronic Structure of Complex Systems*; Phariseau, P., Temmerman, W. M., Eds.; Plenum: New York, 1984.
(20) Andersen, O. K.; Jepsen, O.; Sob, M. In *Electronic Band Structure and its Applications*; Yussouff, M. Ed., Springer-Verlag: Berlin, 1986.
(21) Skriver, H. L. *The LMTO Method*; Springer-Verlag: Berlin, 1984.
(22) Krier, G.; Jepsen, O.; Burkhardt, A.; Andersen, O. K. *TB-LMTO-ASA*, version 4.7.

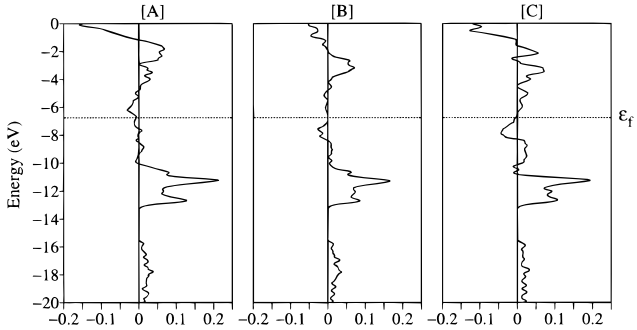


**Figure 7.** Ni−Si COOPs in the TiNiSi structure. The labels ([A],-[B],and [C]) are defined in Figure 1.

transferred from the Ti to the NiSi network are divided almost evenly between the Ni and Si, which have charges of −0.91 and −0.97, respectively. Already we have a large difference between TiNiSi and $BaIn_2$. In $BaIn_2$, the Ba transfers almost all of its electrons to the $In_2$ network (the calculated charge on the Ba was +1.98[1]). Here, the Ti retains a large amount of its electron density.

Another difference between TiNiSi and $BaIn_2$ is seen when we examine the crystal orbital overlap population (COOP)[16,23] curves for the Ni−Si bonds of the 3D4C net, Figure 7. We use the same labels ([B] parallel to the ladders, [C] perpendicular to the ladders, and [A] connecting the ladders) for the three different Ni−Si bond types as we used for the In−In bonds of $BaIn_2$. These are defined above in Figure 1.

If the 3D4C nets of TiNiSi and $BaIn_2$ were electronically similar, we would expect similarly shaped COOP curves for the two systems. Since TiNiSi and $BaIn_2$ are formally isoelectronic (with 32 electrons/unit cell), the Fermi levels should fall in similar regions of the COOP curves. This is not the case. In the In−In COOP curves of $BaIn_2$, the states just below $\epsilon_f$ are strongly bonding along [C], antibonding along [B], and weakly bonding along [A] (Figure 3 in ref 1). Here however, the states just below $\epsilon_f$ in TiNiSi are weakly antibonding along all three Ni−Si bonds. Clearly the Ti atoms are perturbing the electronic structure of the net. We will discuss this below.

Before discussing the perturbations caused by the interstitials, it is important to make one further point about the COOP curves of Figure 7. The region above $\epsilon_f$ in TiNiSi (the states that will be filled as we increase the number of valence electrons on M) is primarily made up of Ti 3d states (Figure 6). These levels have only small contributions from Ni and almost no Si contributions. This region of the DOS is, therefore, essentially nonbonding between Ni and Si. We would not expect the occupation of these states to have a significant impact upon the bonding in the NiSi network. This is very different from the situation in the Zintl compounds related to $BaIn_2$, where addition of extra electrons (beyond 32 electrons/unit cell) populates states that are strongly antibonding within the network.

Figure 8 shows the Ti coordination environment in TiNiSi. The Ti is surrounded by a distorted square pyramid of Si atoms, with two sets of equatorial bonds ([1] and [2] in Figure 8), which span links of the NiSi ladders. Figure 9, showing the COOP curves for bonds from the Ti to the Ni and Si in the 3D4C net, indicates that there are substantial bonding interactions between the Ti atoms and the atoms of the net. The average values of the Ti−Si and Ti−Ni COOPs are 0.224 and 0.054, respectively.

To be able to discuss the magnitude of the Ti−Si and Ti−Ni COOPs in TiNiSi, we need some other COOPs to use as metrics.

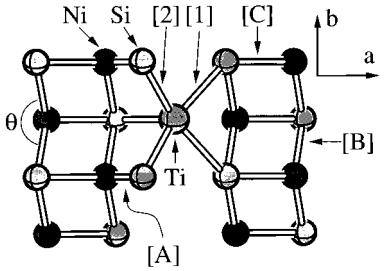


**Figure 8.** Ti coordination environment in TiNiSi.

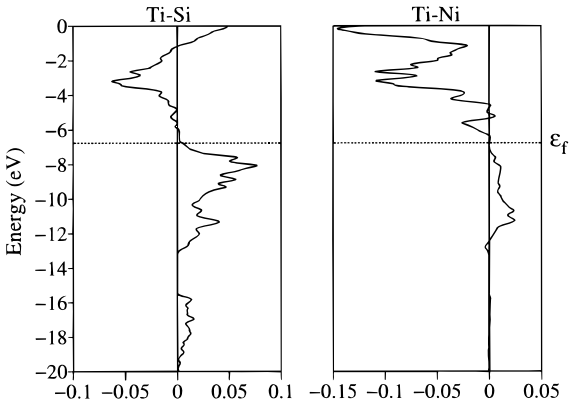


**Figure 9.** Ti−Si and Ti−Ni COOPs in the TiNiSi structure.

We have chosen some binary intermetallics to provide our measuring stick for Ti−Ni and Ti−Si COOPs. One of the polymorphs of TiSi has the FeB structure (space group *Pnma*).[24] The average Ti−Si distance is 2.63 Å, giving a Ti−Si COOP of 0.204. A high-temperature phase of TiNi adopts the CsCl structure (space group $Pm\bar{3}m$),[25] with Ti−Ni distances of 2.61 Å. The Ti−Ni COOP here is 0.232. At lower temperatures, TiNi undergoes a phase change to the TiNi martensite structure (space group $P2_1/m$), with an average Ti−Ni distance of 2.56 Å.[26] The average Ti−Ni COOP in this structure is 0.188.

Comparing the Ti−Si and Ti−Ni COOPs from TiNiSi (0.224 and 0.054 respectively) and distances (2.61 and 2.77 Å) with the values from the binary intermetallics, we see that the Ti−Si interactions are quite strong (stronger, in fact, than the value in TiSi). On the other hand, the Ti−Ni bonds are relatively weak (less than 1/3 of the value in the martensite phase of TiNi and less than 1/4 of the value in the high-temperature, CsCl, phase).

The interstitial Ti atoms in TiNiSi clearly are not innocent of bonding. They retain a significant fraction of their electron density and form strong bonds to the NiSi network. This leads us to expect that the "extra" electrons (those that bring the count to more than 32 electrons/unit cell) as we move along the series M = Ti → Ni in MNiSi are going to be involved in bonds to the NiSi network. This is demonstrated in Table 4, which shows the available average M−Ni and M−Si distances for the MNiSi series. The only large changes here occur in the M−Si distances upon moving from M = Sc to M = Ti. This is the point at which the M atoms become active in bonding to the 3D4C network. Accompanying this shortening of the M−Si bonds is a precipitous drop in the $\vec{b}$ lattice parameter (see Figure 2). The Ti coordination environment in TiNiSi, shown above in Figure 8, provides an easy explanation for this sudden drop in

(23) Hughbanks, T.; Hoffmann, R. *J. Am. Chem. Soc.* **1983**, *105*, 3528.
(24) Brukl, C.; Nowotny, H.; Schob, O.; Benesovsky, F. *Monatsh. Chem.* **1961**, *92*, 781.
(25) Philip, T. V.; Beck, P. A. *J. Metals* **1957**, *9*, 1269.
(26) Michal, G. M.; Sinclair, R. *Acta Crystallogr. B* **1981**, *37*, 1803.

**Table 4.** Average M−Si and M−Ni Distances (Å) for the Members of the MNiSi Family That Have Been Fully Crystallographically Characterized[a]

| M | *R* (M−Si) | *R* (M−Ni) |
|---|---|---|
| Sc | 2.84 | 2.79 |
| Ti | 2.61 | 2.83 |
| V | 2.54 | 2.77 |
| Mn | 2.53 | 2.76 |
| Fe | 2.47 | 2.64 |
| Co | 2.45 | 2.62 |
| Ni | 2.48 | 2.62 |

[a] These numbers were calculated by averaging all M−Si or M−Ni contacts less than 3.0 Å long.

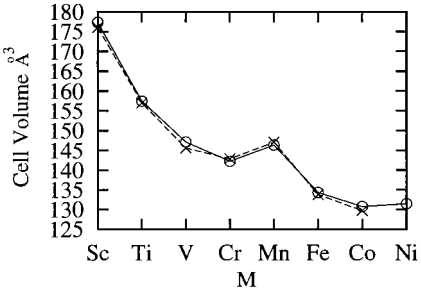


**Figure 10.** Evolution of the volume of the unit cell in MNiSi (solid line) and MCoSi (dashed line) as M is varied.

the length of $\vec{b}$. The Ti−Si bonds (labeled [1] and [2] in Figure 8) fold the ladders, decreasing the angle $\theta$ from 119° in ScNiSi to 105° in TiNiSi. This leads to a shortening of $\vec{b}$ without significantly affecting the lengths of the Ni−Si bonds along the chains; [B] shortens by only 0.01 Å on moving from ScNiSi to TiNiSi.

There are no large changes in the M−Si or M−Ni bond lengths upon moving from Mn to Fe (this is where the sharp change in the $\vec{a}$ and $\vec{c}$ lattice parameters occurs, Figure 2). As we will see below, the cause of the changes in these lengths is the onset of M−M bonding.

### 5. Chair → Boat Transition

The final structural puzzle in the MTSi systems is the change in geometry of the six-membered rings from chair to boat form (shown in Figure 3) as we move from M = Mn to M = Fe in the MNiSi and MCoSi series. This structural change is accompanied by a dramatic (0.88 Å in MNiSi and 0.90 Å in MCoSi) decrease in the length of the $\vec{a}$ lattice vector and a smaller (0.25 Å in MNiSi and 0.32 Å in MCoSi) expansion of $\vec{c}$ (Figure 2). There are similarly dramatic changes in the volume of the unit cell; see Figure 10.

Accompanying these changes is an alteration in the nature of the M−M contacts. Each structure has two close M−M contacts, labeled in **3**.

We will call these "across" for cross-cavity and "between" for the contact between cavities. These lengths for MNiSi and MCoSi are given in Table 5. Compared with the Mn−Mn distance in metallic Mn (2.67 Å) the Mn−Mn distances in both MnNiSi and MnCoSi (in excess of 3.0 Å) are fairly large. In the FeTSi structures, however, there is a large difference in the lengths of the "across" and "between" Fe−Fe contacts. The cross-cavity distances in each of these structures is very long, >3.6 Å. However, the between-cavity distances are quite short, 2.56 and 2.50 Å in FeNiSi and FeCoSi. These bonds, which are about the same length as the Fe−Fe distance in metallic Fe (2.48 Å), give rise to one-dimensional chains of Fe running along the $\vec{a}$ axis. One of these is highlighted with a thick black line in **3**. The presence of these chains of Fe is almost certainly indicative of the formation of Fe−Fe bonds.

**Table 5.** M−M Bond Lengths (Å) in the Later Members of the MNiSi and MCoSi Families

| | MNiSi | | MCoSi | |
|---|---|---|---|---|
| M | M−M (across) | M−M (between) | M−M (across) | M−M (between) |
| Mn | 3.01 | 3.13 | 3.11 | 3.06 |
| Fe | 3.60 | 2.56 | 3.71 | 2.50 |
| Co | 3.56 | 2.54 | 3.65 | 2.49 |
| Ni | 3.44 | 2.59 | | |

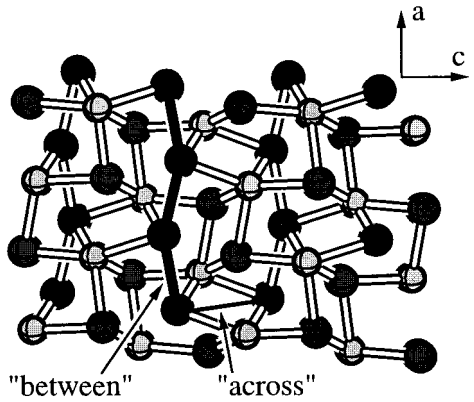


**3**

The most obvious difference between the calculated electronic structures of FeNiSi and TiNiSi is the charge upon the M atom in each compound. In FeNiSi, the Fe, which has a calculated charge of −0.02, is slightly *oxidizing* the NiSi network. On the other hand, in MnNiSi, the Mn, with a charge of +0.45, is *reducing* the NiSi network, just as Ti did in TiNiSi. According to our calculations, the electrons, which are being transferred to the Fe in FeNiSi, are coming from the Si, which has a charge of +0.20 (the remainder of the electrons from the Si end up on the Ni atoms). In MnNiSi, the charge on Si is still slightly negative, −0.10. So, as we move from MnNiSi to FeNiSi, the direction of charge flow changes.

A qualitative plot (adapted from a similar plot in ref 16) showing the evolution of the width of the metal d-block and the position of the Fermi level as we move across the late transition metals, **4**, gives us some insight into what must be going on here.

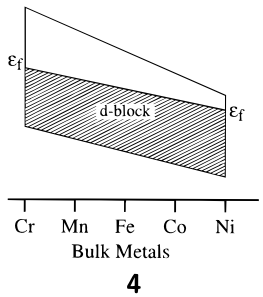


**4**

As we move across the later elements of the first transition series, the position of $\epsilon_f$ gradually drops and the d-block narrows. This comes about because the d orbitals of the metals drop in energy and contract along this series. In our calculations, somewhere in the vicinity of Fe, the M d orbitals are low enough in energy that charge flows from the NiSi network onto the interstitial M atoms. Even if our eHT parameters are somewhat off and the direction of charge flow does not actually reverse,

the general trend should be accurate—as we move across the first transition series, the number of electrons transferred from the M atoms to the NiSi (or CoSi) net will decrease.

The bonding in the NiSi network of FeNiSi is very similar to that in TiNiSi. The Ni−Si COOP curves for FeNiSi (not shown here) are similar to those in Figure 7. The position of $\epsilon_f$ in FeNiSi is slightly higher in the curve (relative to the small region of states that is antibonding along bonds [A], [B], and [C]), but that is to be expected given the larger number of electrons in FeNiSi. The average Ni−Si COOPs are also a fair bit smaller in FeNiSi (0.268, 0.235, and 0.256 for bonds [A], [B], and [C]) than in TiNiSi (0.367, 0.304, 0.306).

The M−M COOP curves for the "across" and "between" bonds in both MnNiSi and FeNiSi are shown in Figure 11. The shapes of the "between" curves are very similar in both structures, though the bonding part in the FeNiSi structure is significantly larger. The average COOPs are as follows: Mn−Mn (across), 0.082; Mn−Mn (between), 0.083; Fe−Fe (across), −0.012; Fe−Fe (between), 0.175. Again, we need a calibration point to be able to interpret these values. A logical choice for this is the M−M COOP in the bulk metals. The M−M COOPs in BCC Mn and Fe are 0.257 and 0.213, respectively. So, the Mn−Mn COOPs in MnNiSi are about 1/3 of the value in bulk Mn, while the Fe−Fe (between) bonds in FeNiSi are almost the same strength as those in bulk Fe. These strong Fe−Fe (between) interactions, which are directed along the $\vec{a}$ axis, have the effect of contracting the $\vec{a}$ lattice parameter. This is the origin of the sharp discontinuity in the plots of $|\vec{a}|$ versus M.

So, we have explained the contraction in the $\vec{a}$ lattice parameter, but the main question still remains—Why do the six-rings change from the chair to the boat form? To answer this question, we need to go back and look at the NiSi network of FeNiSi again, **5**.

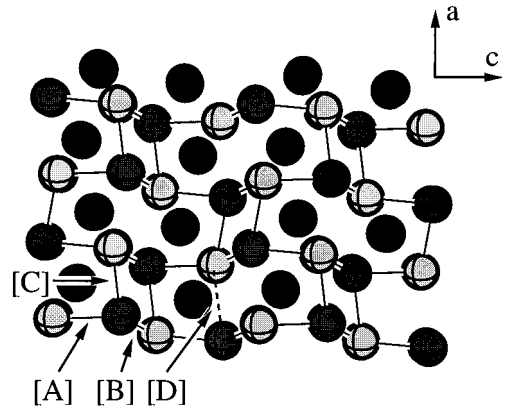


**5**

Here we have labeled one additional Ni−Si contact, [D]. Bond [D] connects the ladders of four-rings along the $\vec{a}$ axis forming, in effect, another connection between the layers of six-rings. In FeNiSi, [D] is quite long, 2.68 Å (compare this with bond [C], the other contact connecting six-rings, which is 2.38 Å long). In MnNiSi, which still has chair form six-rings, contact [D] is considerably longer, 3.66 Å. The average Ni−Si COOP for bond [D] (COOP curve not shown here) in FeNiSi is 0.064. While this is around one-quarter of the COOP values in the 3D4C net, it is probably still responsible for changing the shape of the six-rings.

If the shortening of bond [D] were to continue until it was about the same length as bond [C], a fascinating three-dimensional *five*-connected network would result, **6**.

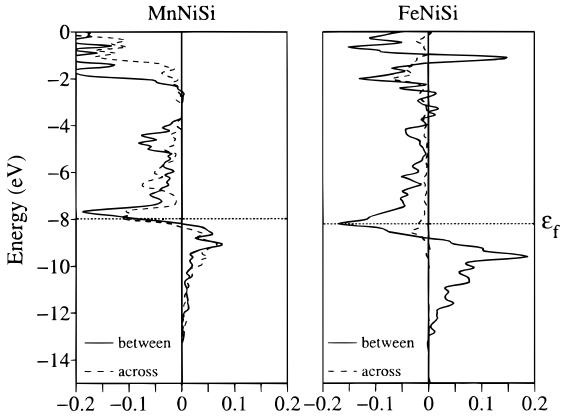


**Figure 11.** M−M COOPs in the MnNiSi and FeNiSi structures. The labels "across" and "between" are defined in the text.

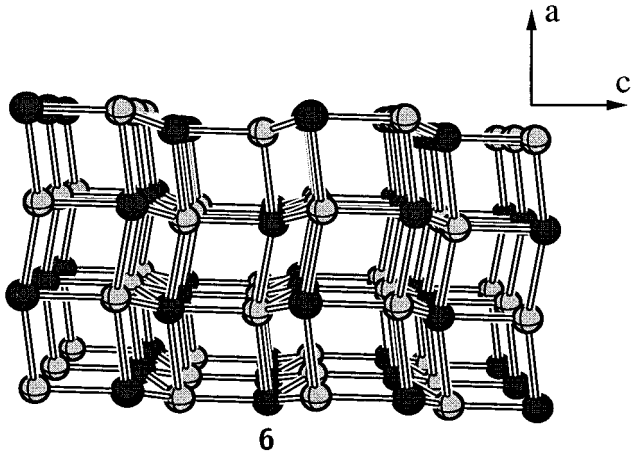


**6**

This NiSi net is a distorted form of the TSi network found in the ZrBeSi (or $Ni_2In$) phases of FeCoSi and CrNiSi, as well as a high-temperature form of MnCoSi.[2] This network, composed of planar sheets of six-membered rings connected along the $\vec{c}$ axis, is shown in **7**.

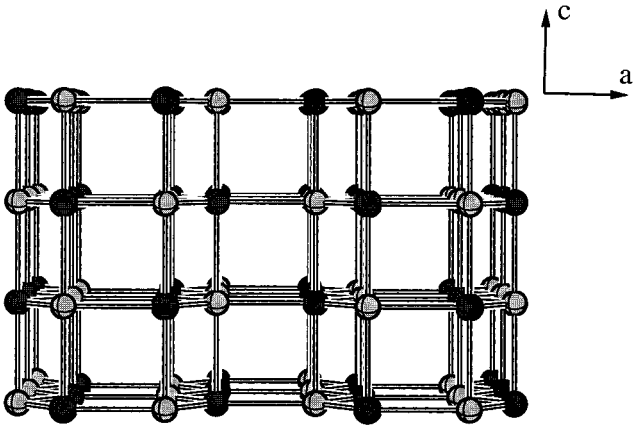


**7**

The Ni−Si COOP curves for an idealized (bonds [C] and [D] set to have equal length) version of the 3D5C network in **6** are shown in Figure 12. The electron-filling in Figure 12 is set to make the network neutral, 16 electrons/unit cell in our way of counting (Ni:0 + Si:4 = 4 × 4 formula units/cell → 16 electrons/cell). This is very close to the count on the NiSi network of FeNiSi (where only 0.02 electrons/formula unit are transferred to the Fe atoms). If we were to reduce this 3D5C

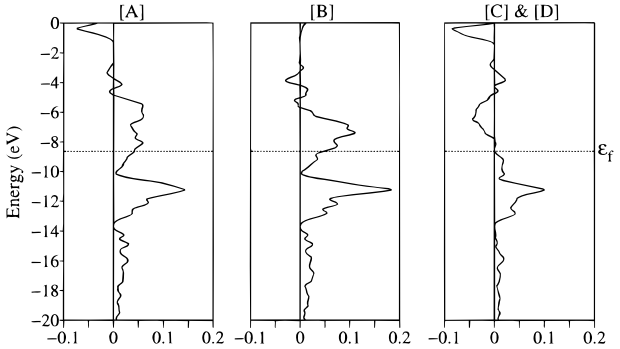


**Figure 12.** Ni−Si COOPs for the hypothetical NiSi network shown in **6**. The Fermi level shown is appropriate for the neutral network.

network, as happens in the early members of the MNiSi family, the states that would be populated are those above $\epsilon_f$ in Figure 12. These levels are bonding along [A] and [B] but antibonding along [C] and [D]. So, reducing the 3D5C network would weaken bonds [C] and [D]. The network can lessen the unfavorable impact of this population of antibonding states in two simple ways. The first, breaking the interlayer bonds entirely, leaves us with three-coordinate Si and Ni atoms in the layers of boat form six-rings. Given silicon's well-known reluctance to form double bonds and tendency toward high connectivity, this does not seem very likely. The other possibility is to lengthen *one* of the interlayer contacts, say bond [D], and shorten the other. This leads us to the 3D4C net actually observed in the MNiSi structures.

So upon moving from MnNiSi to FeNiSi, M−M bonding along the $\vec{a}$ axis becomes important. This bonding contracts the $\vec{a}$ axis, shortening contact [D] to the point that a bond starts to form. The six-rings then distort into the boat form to allow [D] to be maximally bonding.

### 6. Existence of MNiSi and MCuSi Phases

None of the results presented so far account for the strange difference between the MNiSi (M = Sc, Ti, V, Cr, Mn, Fe, Co, Ni) and MCoSi (M = Sc, Ti, V, Cr, Mn, Fe, Co) families of compounds and the MCuSi series (which only exists for M = Sc and Ti). In fact, we have presented several arguments that indicate that this is not simply explained in terms of a bonding analysis. Calculations upon hypothetical MCuSi phases indicate that the small spatial extent of the Cu 3d orbitals compared to those of Ni and Co likely is quite important. These results will not be presented here, as a far simpler model provides an adequate explanation. The key to understanding this difference is to change our perspective slightly. We have shown that, once we move past M = Ti in the MNiSi series, it is reasonable to assume that there will be bonding between M and the Ni and Si. Using this, we adopt the view that MTSi is a M−T intermetallic phase with intercalated Si "impurities". Now consider the existence of stable M−T phases (no Si at all),[2] shown in Table 6. This is very suggestive; in *every* case, an MTSi phase exists only if a corresponding M−T phase exists. So, if M and T are incompatible, MTSi will not form.

It is by no means straightforward to explain the stabilities of metal alloys, and we make no attempt here to do so. However, there is a wonderfully simple and effective semiempirical scheme that was developed for just this problem by A. R. Miedema more than 20 years ago. [27−30] In their simplest form,

(27) de Boer, F. R.; Boom, R.; Mattens, W. C. M.; Miedema, A. R.; Niessen, A. K. *Cohesion in Metals: Transition Metal Alloys*; Cohesion and Structure Series; North-Holland: New York, 1988.

**Table 6.** Existence of M−T and MTSi Phases[a]

| | M | | | | | |
|---|---|---|---|---|---|---|
| T | Co | | Ni | | Cu | |
| Sc | Y | **Y** | Y | **Y** | Y | **Y** |
| Ti | Y | **Y** | Y | **Y** | Y | **Y** |
| V | Y | **Y** | Y | **Y** | N | **N** |
| Cr | Y | **Y** | Y | **Y** | N | **N** |
| Mn | Y | **Y** | Y | **Y** | N | **N** |
| Fe | Y | **Y** | Y | **Y** | N | **N** |
| Co | Y | **Y** | Y | **Y** | N | **N** |

[a] The first entry in each column indicates whether M−T phases are known; the second (in bold face) indicates whether MTSi phases are known. Y = phase exists; N = phase does not exist. These data, with the exception of some of the MTSi phases, are taken from ref 2.

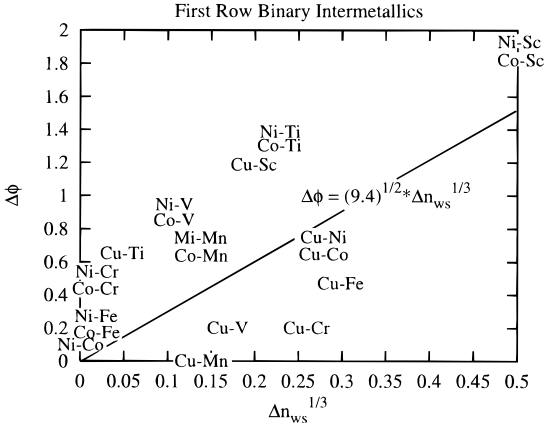


**Figure 13.** Miedema plot for the M−T pairs of Table 6. The parameters used in this plot are given in the text.

the Miedema rules use two parameters for each transition metal: $\phi^*$, a measure of the work function or electronegativity of the metal; $n_{ws}$, the electron density at the edge of the Wigner−Seitz cell in the pure metal. This model is developed in great depth in ref 27, so only the bare essentials will be covered here.

Continuing to stay at the simplest possible level of the Miedema model, we can determine if stable compounds can exist between metals M and T by plotting the difference in their $\phi^*$ values versus the difference in the cube root of the values of $n_{ws}$. If the plotted point lies above the line

$$|\Delta\phi^*| = \sqrt{9.4}\,|\Delta n_{ws}^{1/3}| \qquad (1)$$

then M−T phases should exist. If the point lies below the line, M−T phases are not predicted to be stable. The origins of the form of this relationship and the magic $\sqrt{9.4}$ premultiplier are given in the publications describing the method. A Miedema plot for the M−T pairs of Table 6 is shown in Figure 13. The parameters used to construct this plot (taken from ref 27) are given below in Table 7. Figure 13 gets the existence of the M−T phases with which we are concerned exactly right.

Before discussing some reasons why Cu is so different from Ni and Co, it is worthwhile to spend a little time on the physical significance of the parameters in the Miedema plot and the form of eq 1. Miedema's rules are based on a so-called "cellular" or "macroscopic atom" model of metals. A bulk metal is broken down into the Wigner−Seitz cells around each atom. Each of

(28) Miedema, A. R.; de Châtel, P. F. In *Theory of Alloy Phase Formation*; Bennet, L. H., Ed.; Met. Soc. AIME: Warrendale, PA, 1979; p 344.
(29) Miedema, A. R.; de Boer, F. R.; de Châtel, P. F. *J. Phys. F* **1973**, *3*, 1558.
(30) Miedema, A. R. *J. Less-Common Met.* **1973**, *32*, 117.

**Table 7.** Parameters Used in the Miedema Analysis[a]

| | Sc | Ti | V | Cr | Mn | Fe | Co | Ni | Cu |
|---|---|---|---|---|---|---|---|---|---|
| $\phi^*$ | 3.25 | 3.80 | 4.25 | 4.65 | 4.45 | 4.93 | 5.10 | 5.20 | 4.45 |
| $n_{ws}^{1/3}$ | 1.27 | 1.52 | 1.64 | 1.73 | 1.67 | 1.77 | 1.75 | 1.75 | 1.47 |

[a] All parameters are taken from ref 27.

these cells has some electron density at its boundaries ($n_{ws}$) and a certain electronegativity/work function ($\phi^*$). When we combine two unlike metals to form an intermetallic compound (alloy), there must be some charge flow between cells in order to reach an "electronic equilibrium" in the alloy. If the two metals have very different electronegativities, then a significant amount of charge will flow from the less electronegative metal to the metal with a higher electronegativity. This is a stabilizing interaction (electrons flowing from higher energy to lower). However, if there is a significant mismatch in the $n_{ws}$ values, then each cell must either expand or contract to reach the equilibrium value. This "resizing" of atoms is not a favorable thing. So, what we want in order to form a stable intermetallic is a large $|\Delta\phi^*|$ combined with a small $|\Delta n_{ws}|$.

Table 7 shows the parameters used to construct Figure 13. Ni is the most electronegative of the first-row transition metals (on this scale at least) and has about the same electron density as the other first-row metals. This gives rise to sizable $|\Delta\phi^*|$ values while $|\Delta n_{ws}^{1/3}|$ is small. Co is similar to Ni, with a value of $\phi^*$ that is only slightly smaller and the same $n_{ws}^{1/3}$ value. The story with Cu is, however, completely different. Cu has a middling electronegativity and a smaller $n_{ws}^{1/3}$ value than all other first-row transition metals with the exception of Sc. So, $|\Delta\phi^*|$s involving Cu are relatively small in comparison with the large $|\Delta n_{ws}^{1/3}|$ that it gives. Consequently, Cu does not form stable phases with most other first-row transition metals. This instability of M−Cu phases (combined with the relatively close M−T contacts in the MTSi structures) leads to the instability of MCuSi phases with most first-row transition metals.

In some cases, however, nature is quite clever about finding ways around problems such as phase instabilities. For instance, Cu and Nb do not form a stable binary intermetallic. However, the phase $Cu_4Nb_5Si_4$, which has almost the 1:1:1 stoichiometry of NbCuSi, exists.[31] A glance at the crystal structure of $Cu_4Nb_5Si_4$, Figure 14, shows how this is possible.

The structure has $Nb_5Si_4$ chains with Cu atoms segregated into the interstitial regions. The closest Cu−Nb contacts are 2.91 Å, well beyond the sum of the covalent radii, 2.51 Å. Contrast this with the Cu−Cu contacts within the cavities, which are as short as 2.61 Å. This segregation of Cu into the regions between the $Nb_5Si_4$ needles has two effects. First, it keeps the incompatible Cu and Nb atoms away from each other, and second, it allows Cu−Cu and Cu−Si bonds to form between the needles. These bonds hold the structure together.

## 7. Conclusions

We approached the study of the MTSi phases seeking the answers to a number of questions.

1. How can the TiNiSi structure type accommodate the hugely varying number of valence electrons in the MNiSi (M = Sc, Ti, V, Cr, Mn, Fe, Co, Ni) and MCoSi (M = Sc, Ti, V, Cr, Mn, Fe, Co) series?

2. What is the origin of the structural change in both the MNiSi and MCoSi series at M = Fe?

3. Why does the MCuSi series stop at M = Ti?

The answers to these questions, as best as we can see them now, are as follows.

1. The states that get filled with the extra electrons in these MTSi structures are essentially nonbonding within the TSi network. So, in contrast to $BaIn_2$ and related structures, the population of these states does not significantly affect the stability of the 3D4C network. As we move across the MTSi series from M = Sc to M = Ni, the added valence electrons go into M−Si bonds and, once we reach M = Fe, M−M bonds.

2. The structural change at M = Fe is brought on by the formation of M−M bonds along the $\vec{a}$ axis. These bonds contract the $\vec{a}$ lattice vector, which brings the layers of six-rings closer together. The resulting close Ni−Si contacts along contact [D] (**5**) distort the geometry of the six-rings to maximize this new interaction.

3. The stability of the various MTSi phases can be accounted for in terms of the stability of the corresponding MT phases using Miedema's rules. While Ni and Co form both stable intermetallics and MTSi phases with all the other first-row transition metals, Cu, which does not form intermetallic phases with any of the first-row transition metals other than Sc and Ti, cannot form MCuSi phases beyond M = Ti.

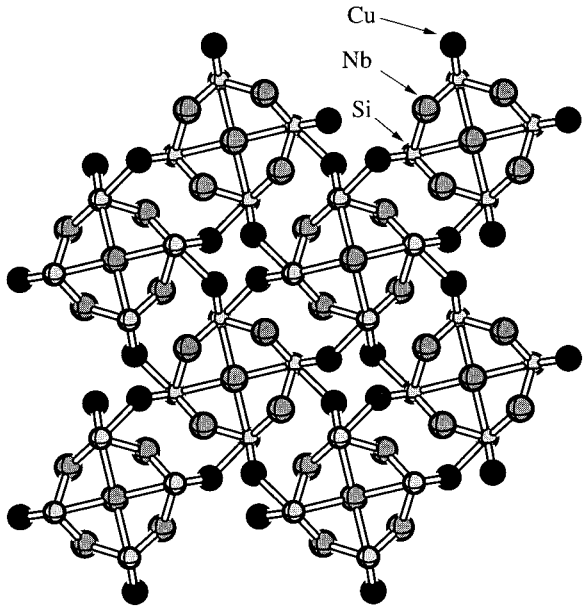


**Figure 14.** A view of the crystal structure of $Cu_4Nb_5Si_4$.

**Table 8.** Parameters Used in the Extended Hückel Calculations

| atom | orbital | $H_{ii}$ (eV) | $\zeta_1$ | $\zeta_2$ | $C_1$ | $C_2$ |
|---|---|---|---|---|---|---|
| Ti | 3 | −5.9 | 4.550 | 1.400 | 0.4206 | 0.7839 |
| | 4s | −6.3 | 1.500 | | | |
| | 4p | −3.2 | 1.500 | | | |
| Mn | 3d | −8.7 | 5.150 | 1.700 | 0.5140 | 0.6930 |
| | 4s | −7.5 | 1.800 | | | |
| | 4p | −3.8 | 1.800 | | | |
| Fe | 3d | −9.2 | 5.350 | 1.800 | 0.5366 | 0.6678 |
| | 4s | −7.6 | 1.900 | | | |
| | 4p | −3.8 | 1.900 | | | |
| Co | 3d | −9.7 | 5.550 | 1.900 | 0.5550 | 0.6678 |
| | 4s | −7.8 | 2.000 | | | |
| | 4 | −3.8 | 2.000 | | | |
| Ni | 3d | −10.5 | 5.750 | 2.000 | 0.5683 | 0.6292 |
| | 4s | −9.0 | 2.100 | | | |
| | 4p | −4.2 | 2.100 | | | |
| Si | 3s | −17.3 | 1.383 | | | |
| | 3p | −9.2 | 1.383 | | | |

(31) Ganglberger, E. *Monatsh. Chem.* **1968**, *99*, 549.

## Appendix: Computational Details

All extended Hückel calculations were carried out using a program written by one of the authors (G.L.).[32] The parameters used in the extended Hückel calculations are given in Table 8. All parameters except those for Ni were taken from a standard set.[33] The parameters used for Ti, Mn, Fe, and Co are those appropriate for the bulk metal. The Ni $H_{ii}$s were adjusted using a charge-iteration procedure. The Ni $\zeta$ values are from the Alvarez Ni metal parameters.

The *k*-point meshes used for reciprocal space integrations were generated within the irreducible wedge of the first Brillouin zone using the method of Ramirez and Böhm.[34] The meshes used contained 27 (all MTSi structures and TiSi), 56 (BCC Fe and Mn), 84 (TiNi in the CsCl structure), and 108 (TiNi in the TiNi structure) *k*-points. All calculations were checked for convergence with respect to the *k*-point sampling.

**Acknowledgment.** R.H. and G.L. are grateful to the National Science Foundation for its support of their work through Research Grant CHE 94-08455. They also thank Silicon Graphics for their generous donation of the computer hardware that was used in this work. J.E. gratefully acknowledges the support of his research by the Deutsche Forschungsgemeinschaft and the Fonds der Chemischen Industrie.

**Supporting Information Available:** Tables listing lattice constants, positional parameters, percentage main phase, $R_{wp}$, and $R_{exp}$ values for all reported compounds (1 page). Ordering information is given on any current masthead page.

IC980223E

(32) Landrum, G. A. *YAeHMOP*, 1997. Freely available on the World Wide Web at URL: http://overlap.chem.cornell.edu: 8080/yaehmop.html.
(33) Alvarez, S. Unpublished results, 1993.
(34) Ramirez, R.; Böhm, M. C. *Int. J. Quantum Chem.* **1988**, *34*, 571.